Orthogonal delay-Doppler division Multiplexing for underwater communication systems

Yixuan Xie*, *Member, IEEE*, Jinhong Yuan*, *Fellow, IEEE*, Peng Chen†, *Member, IEEE*,
Yue Rong†, *Senior Member, IEEE*, Andrew Zhang**, *Senior Member, IEEE*
*The University of New South Wales, †Curtin University, **University of Technology Sydney
{yixuan.xie, j.yuan}@unsw.edu.au, {peng.chen, y.rong}@curtin.edu.au, Andrew.Zhang@uts.edu.au

***Abstract*—Reliable communications in underwater scenarios are one of the biggest challenges due to the channel's severe time-varying multipath effects. Transmission waves typically become highly dispersed in time and frequency because of the Doppler effect and multipath signal delays, leading to a complex transceiver design. In recent years, delay-Doppler domain modulation schemes, such as orthogonal time frequency space (OTFS) and orthogonal delay-Doppler division multiplexing (ODDM), have received significant attention to address the challenge of waveform design for doubly dispersive channels. These modulation techniques deal with doubly dispersive channels by designing signal waveforms coupled well with the channels' delay-Doppler variations. Compared with conventional orthogonal frequency division multiplexing (OFDM) systems, OTFS and ODDM are more efficient in alleviating inter-carrier interference (ICI) in doubly dispersive channels for which a reliable underwater communication link can be maintained. Motivated by this, our work investigates the feasibility of ODDM modulation in underwater acoustic communication systems. We first present the proposed structure of the transmission frame for the underwater communication scenario, followed by the signal preprocessing and post-processing steps of the ODDM scheme, such as channel estimation and detection. The software-defined radio (SDR) implementation of ODDM is also described for practical experimental setups. Initial tank experiment results for ODDM with different detection methods are provided.**

***Index Terms*—ODDM, delay-Doppler, software-defined radio (SDR).**

I. Introduction

UNDERWATER acoustic communication (UAC) plays a pivotal role in a wide range of essential marine applications. It facilitates data transmission in underwater environments where traditional radio waves are ineffective. UAC is crucial for various activities, including oceanographic research, environmental monitoring, underwater exploration, and the development of marine renewable energy systems. The ability to maintain reliable communication in such environments is vital for advancing scientific knowledge, ensuring national security, and managing marine resources sustainably.

The underwater communication channel presents unique challenges distinct from terrestrial and aerial communication systems. These channels are characterized by severe multipath propagation, high attenuation, and limited bandwidth, leading to significant signal degradation. Channel variability is further influenced by environmental factors such as salinity, temperature, and depth, all of which can cause fluctuations in signal strength and quality. Additionally, the Doppler effect, resulting from the relative motion between the transmitter and receiver, complicates signal stability. Moreover, the slower speed of sound in water compared to radio wave leads to longer delays and increased latency. These challenges necessitate advanced modulation schemes, error correction methods, and adaptive protocols to ensure reliable data transmission.

Orthogonal Frequency Division Multiplexing (OFDM) is a widely-used multicarrier modulation technique in wireless communications, known for its robustness against frequency-selective fading in wideband channels. Nonetheless, highly time-dispersive channels can disrupt the orthogonality between OFDM subcarriers, which may lead to substantial performance degradation. This loss of orthogonality results in inter-carrier interference (ICI), negatively impacting the system's ability to reliably transmit and receive data, especially in channels with strong Doppler effect, such as underwater acoustic channels. Motivated by the challenges, recent advances in modulation techniques, such as Orthogonal Time Frequency Space (OTFS) [1], [2] and Orthogonal Delay-Doppler Division Multiplexing (ODDM) [3]–[7], have gained significant attention. Recent studies have shown that the DD domain modulated signal is coupled with a relatively stable and compact delay-Doppler (DD) domain channel model. This enables simpler channel estimation and more accurate detection at the receiver side, allowing for superior performance over OFDM in high-Doppler environments.

Software-defined radio (SDR) has emerged as a flexible platform that enables rapid prototyping of fully agile, intelligently adaptive, and reconfigurable networking devices to accommodate and test novel wireless networking protocols for communication systems. Unlike traditional hardware radio communication systems, an SDR system is a communication platform where most or all of the physical layer protocols and algorithms are performed in software. Many works on the hardware design and implementation of digital communication systems, including UAC systems, have been studied in the literature, for instance, [8]–[11]

In this work, we present an SDR-based design of ODDM transceiver systems using Universal Software Radio Peripheral (USRP) SDR platforms. More specifically, we describe the transmitter process, including the frame structure of an ODDM frame, followed by the receiver process, which covers Doppler scale compensation, channel estimation, and detection. The performance of the designed ODDM system is tested in a

laboratory water tank. Experimental results show that the ODDM system yields higher bit rate and bandwidth efficiency compared to the OFDM system with similar configurations.

The paper is organized as follows: Section II introduces the system model of ODDM for underwater acoustic channels. In Section III, the SDR implementation of the ODDM transceiver is discussed. Before concluding the work in Section V, Section IV contains the experimental results of the designed ODDM systems.

II. ODDM System for UWA channels

Consider an ODDM frame spanning a duration of NMT_s, where it transmits M multi-carrier ODDM symbols staggered by T/M and each ODDM symbol has N subcarriers spaced by $1/NT$. Let $T_s = T/M$ be the sampling period. The resolutions of the delay (time) and Doppler (frequency) are $T_s = T/M$ and $1/MNT_s = 1/NT$, respectively. An ODDM frame carries MN symbols $\{X[m,n]\}_{0\le m\le M-1, 0\le n\le N-1}$, where $[m,n]$ indicates the n-th subcarrier of the m-th ODDM symbol.

For the m-th ODDM symbol, using the N-point IDFT, the rows of $X[m,n], 0 \le n \le N-1$, are transferred to time domain (TD) samples

$$\hat{x}[m,\bar{n}] = \frac{1}{\sqrt{N}} \sum_{n=0}^{N-1} X[m,n] e^{j2\pi \frac{n\bar{n}}{N}}, 0 \le \bar{n} \le N-1. \quad (1)$$

The discrete-time samples of each ODDM symbol are up-sampled by the factor of M. Then these samples from all of the M ODDM symbols are staggered to form the baseband signal $\{x[k]\}$ of an ODDM frame as follows

$$x[k] = \hat{x}\left[[k]_M, \left\lfloor \frac{k}{M} \right\rfloor\right] 0 \le k \le NM-1, \quad (2)$$

where $[k]_M \triangleq \mod(k,M)$ and $\lfloor\cdot\rfloor$ is the floor function. Such a staggering process is essentially the time-multiplexing of M ODDM symbols with spacing T_s.

To mitigate the inter-frame-interference between neighbouring ODDM frames, a cyclic prefix (CP) of length $L_{cp} < M$ is employed, and the final ODDM frame is given by

$$\hat{x}[k] = \begin{cases} x[MN+k], & k = -L_{cp}, \cdots, -1, \\ x[k], & k = 0, \cdots, MN-1. \end{cases} \quad (3)$$

With the above IDFT-based approximate implementation, the generated passband signal is given by

$$s_{\mathbf{p}}(t) = \mathrm{Re}\left\{ \left[\sum_{m=0}^{M-1} \sum_{n=0}^{N-1} X[m,n] a_{m,n}(t) \right] e^{j2\pi f_c t} \right\}, \quad (4)$$

where f_c is the carrier frequency and

$$a_{m,n}(t) = \sum_{\bar{n}=0}^{N-1} e^{j2\pi \frac{n\bar{n}}{N}} a(t - \bar{n}T - mT_s), \quad (5)$$

is the practical delay-Doppler orthogonal pulses (DDOP) characterized by a truncated square-root Nyquist pulse $a(t)$ [3].

The received passband signal is then given by

$$r_{\mathbf{p}}(t) = \int_{-\infty}^{\infty} s_{\mathbf{p}}(t-\tau) h(\tau,t) d\tau, \quad (6)$$

where the impulse response of the time-varying multipath channel, which is a common model for UAC channels, is given by

$$h(\tau,t) = \sum_{l=1}^{L} h_l(t) \delta(\tau - \tau_l(t)). \quad (7)$$

Here, L denotes the total number of paths. Let $\tau_l(t) \approx \tau_l - \alpha_l t$ be the approximation of the time-variant delay of path l, which is a time-scaling commonly exsits in wideband systems. The scaling factor α_l is known as the Doppler scale of the l-th path. Assume the gain h_l of each path is constant over the period $T_s = T/M$, and a constant Doppler scale α for all the paths. Then,

$$h(\tau,t) = \sum_{l=1}^{L} h_l \delta(\tau - \tau_l + \alpha t). \quad (8)$$

As a result, the received passband signal can be represented as

$$r_{\mathbf{p}}(t) = \sum_{l}^{L} h_l s_{\mathbf{p}}((1+\alpha)t - \tau_l) + z_{\mathbf{p}}(t), \quad (9)$$

where $z_{\mathbf{p}}(t)$ is the passband noise.

After the down-convertion, the baseband signal $r_{\mathbf{b}}(t)$ at the receiver can be obtained as

$$\begin{aligned} r_{\mathbf{b}}(t) &= e^{-j2\pi f_c t} r_{\mathbf{p}}(t) \\ &= e^{-j2\pi f_c t} \\ &\left(\sum_{l=1}^{L} h_l \left(\left[\sum_{m=0}^{M-1} \sum_{n=0}^{N-1} X[m,n] a_{m,n}(t - \tau_l + \alpha t) \right] e^{j2\pi f_c (t - \tau_l + \alpha t)} \right) \right. \\ &= \sum_{l=1}^{L} h_l e^{-j2f_c(\alpha t - \tau_l)} \\ &\times \left(\sum_{m=0}^{M-1} \sum_{n=0}^{N-1} X[m,n] a_{m,n}(t - \tau_l + \alpha t) \right) + z_{\mathbf{b}}(t), \end{aligned} \quad (10)$$

where $z_{\mathbf{b}}(t)$ is the baseband noise. It can be seen from (10) that in addition to the delay τ_l and the Doppler shift αf_c, the waveform $s_{\mathbf{p}}(t)$ is compressed when $\alpha > 0$ or dilated if $\alpha < 0$, which needs to be taken care of before the receiver process starts.

III. SDR implementation of ODDM Transceiver

While the concept of ODDM modulation for UWA channels is discussed in the previous section, the digital implementation of the ODDM transceiver is introduced in this section. Fig. 1 illustrates the overall SDR transceiver architecture of the designed ODDM system. The USRP platform used is the N210 model, which is an FPGA-based SDR platform consisting of a pair of digital up and digital down converters (DUC/DDC), dual 100 MS/s ADC modules, and dual 400 MS/s DAC modules. A pair of low-frequency band front-ends, LFTX/LFRX daughterboards, are used for transmitting and receiving the signal at a frequency range of 0-30 MHz. Each USRP device is connected to a host computer, which is used

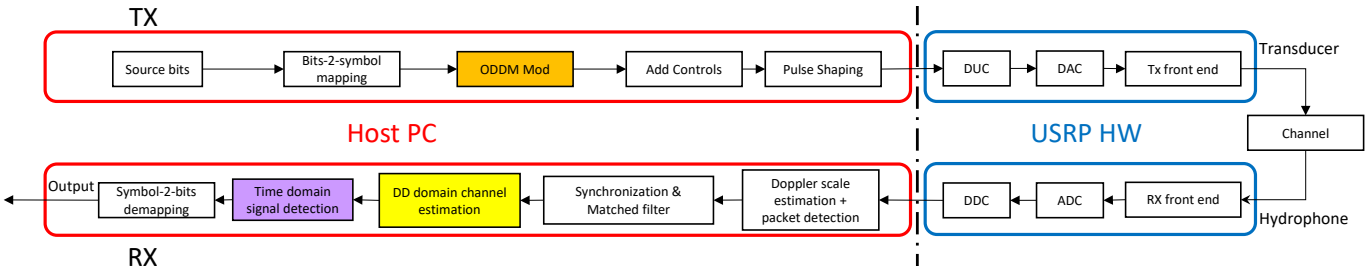

Fig. 1. SDR transceiver architecture.

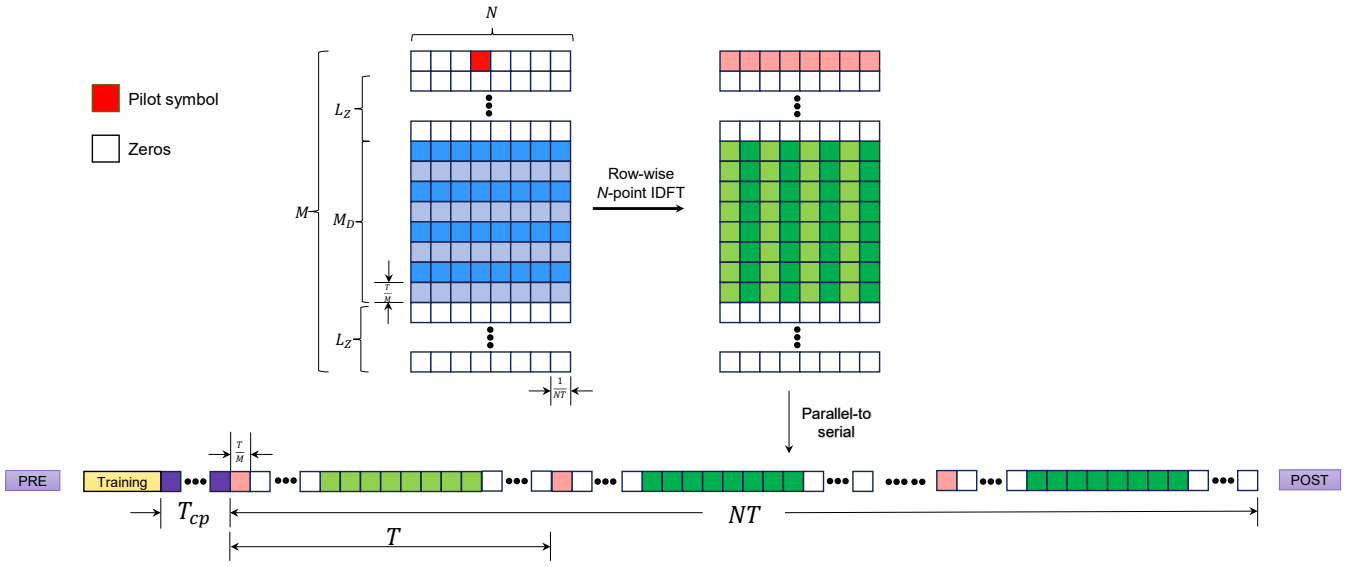

Fig. 2. ODDF frame structure

to perform baseband signal modulation and demodulation at the transmitter and receiver sides, respectively.

A. Transmitter process

It can be seen that for each ODDM data frame, the transmitter first generates a binary sequence $\mathbf{b}$ of length L_b. This binary sequence is mapped to QAM symbols resulting the symbol sequence $\mathbf{d}$ of length $L_d = L_b/q = \theta MN$, where q denotes the modulation order and θ indicates the number of ODDM frames for the transmission.

Assume $\theta = 1$, to perform the ODDM modulation, the symbol sequence $\mathbf{d}$ is converted into an $M \times N$ 2-D data block $X[m,n]$, where N is some positive integer, and $M = M_D + 2L_Z + M_P$ denotes the number of ODDM symbols. The parameters M_D, M_P and L_Z denote the number of ODDM data, pilot and zero symbols, respectively. Let $M_P = 1$. The ODDM pilot symbol is inserted at $m = 0$ with the structure of

$$X[0,n] = \begin{cases} 0 & 0 \le n \le \lceil N/2 \rceil - 1 \\ \sqrt{E_p} x_p & n = \lceil N/2 \rceil \\ 0 & \lceil N/2 \rceil \le n \le N-1 \end{cases}, \quad (11)$$

where x_p and E_p denote the pilot symbol and its symbol energy. Next, a block of $L_Z \times N$ zeros are padded below the ODDM pilot symbol and the ODDM data symbols. Hence, the proposed ODDM system is also known as the zero-padded ODDM system.

By performing row-wise N-point IDFT operation, the data block $X[m,n]$ is transformed to time domain data block $x[m,n]$ of size $M \times N$. The parallel-to-serial operation is performed to vectorize $x[m,n]$ into a length MN vector $x[k], 0 \le k \le MN-1$ by concatenating N columns of $x[m,n]$. Finally, the CP-extended sequence $\hat{x}[k]$ is obtained by attaching the last L_{cp} symbols of $x[k]$ to the beginning. Let $L_{cp} = L_Z$. In the proposed zero-padded ODDM system, this is equivalent to adding L_Z zeros to the start of the sequence.

To enhance the reliability of the transmission, control sequences need to be added to mitigate channel effects at the receiver. In the proposed design, a preamble and postamble of a transmission frame are used to mitigate the Doppler scaling effect at the receiver side. In addition, we use a training sequence to perform frame synchronization at the receiver side. The transmission frame structure of the proposed ODDM system is illustrated in Fig. 2.

Before the ODDM frame is send off to the USRP hardware for tranmission, a digital pulse shaping is performed. Since $\hat{x}[k]$ is a vector of length $MN + L_{cp}$, the genertion of

passband waveform at the transmitter can be implemented approximately by applying the $g_{tx}(t)$-based sample-wise pulse shaping (filtering) as

$$s_{\mathbf{p}}(t) = \mathrm{Re}\left\{ \left[\sum_{k=-L_{cp}}^{MN-1} \hat{x}[k] g_{tx}(t - kT_s) \right] e^{j2\pi f_c t} \right\}, \quad (12)$$

where $g_{tx}(t) = a(t)$. In the proposed system, the root-rasised cosine function is adopted as the coefficients of the pulse shaping filter. The discrete-time samples at the filter outputs is then digital up-converted (DUC) to the passband with the desired carrier frequency f_c. The passband signal is then fed into the digital-to-analogue converter (DAC), where the outputs are ready to be transmitted over the physical channel through the transceducer that connects to the the LFTX daughterboard.

B. Receiver process

The processing steps at the receiver side are shown in the lower chain of Fig. 1. The analogue passband signal is first picked up by the hydrophone, fed to the high-speed analogue-to-digital converter (ADC) via LFRX daughterboard, followed by a digital down-converted (DDC) to bring the signal back to baseband. The output of the DDC is the discrete-time baseband samples $r_{\mathbf{b}}[k] = r_{\mathbf{b}}(kT_s)$ ready for the receiver processes, where $T_s = T/M$ is the sampling period.

1) Mitigation of Doppler scaling: Upon the reception of the signal at the receiver, the first step is to perform compensation for the Doppler scaling effect. To estimate the Doppler scale factor α, the preamble and postamble of the transmission frame are used. By performing a cross-correlation of the received signal $r_{\mathbf{b}}[k]$ with the known preamble and postamble, we obtain $\hat{T}_{rx}$, which measures the time difference between the correlation peaks at the preamble and postamble. The position of the two peaks indicates the boundary position of the preamble and postamble[1]. Furthermore, the time duration T_{tx} of the frame at the transmitter side is deterministic. Thus, the receiver estimates the Doppler scale $\hat{\alpha}$ by

$$\hat{\alpha} = \frac{T_{tx}}{\hat{T}_{rx}} - 1. \quad (13)$$

Then $r_{\mathbf{b}}[k]$ is resampled with a resampling factor of $\hat{\alpha}$. Since the USRP hardware directly digitize the analogue signal when the signal is received, the resampling is performed on the discrete baseband sample sequence $r_{\mathbf{b}}[k]$. Hence,

$$\hat{r}_{\mathbf{b}}[k] = r_{\mathbf{b}}\left(\frac{kT_s}{1+\hat{\alpha}}\right). \quad (14)$$

Conceptually, the resampling process on continouse-time signal is given by

$$\hat{r}_{\mathbf{b}}(t) = r_{\mathbf{b}}\left(\frac{t}{1+\hat{\alpha}}\right)$$

[1]In our ODDM system, the boundary of the preamble and postamble is also used to determine whether a full transmission frame has been received. Hence, it triggers the subsequent signal processing modules.

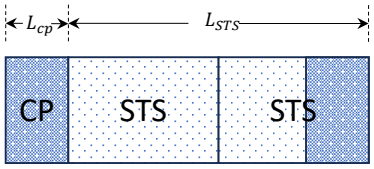

Fig. 3. Structure of the synchronization sequence

$$= \sum_{l=1}^{L} h_l e^{-j2f_c(\frac{\alpha}{1+\hat{\alpha}}t - \tau_l)} \times \left(\sum_{m=0}^{M-1} \sum_{n=0}^{N-1} X[m,n] a_{m,n} \left(\frac{1+\alpha}{1+\hat{\alpha}} t - \tau_l \right) \right) + \hat{z}_{\mathbf{b}}(t) \quad (15)$$

where $\hat{z}_{\mathbf{b}}(t)$ is the additive noise in baseband. The target is to estimate $\hat{\alpha}$ as close to α as possible such that $(1+\alpha)/(1+\hat{\alpha}) \approx 1$, leaving a residue Doppler effect of $e^{-j2f_c(\frac{\alpha}{1+\hat{\alpha}}t - \tau_l)}$, which is a small frequency shift of the carrier frequency f_c.

2) Matched filter and Synchronization: The resampled baseband signal $\hat{r}_{\mathbf{b}}[k]$ is feed through a matched filter, $g_{rx}(t) = g_{tx}(-t)$, which is identitcal to the pulsed shaping filter used at the transmitter side if root-raised cosine function is considered.

To locate the start of the frame, correlator-based frame synchronization technique is performed on the length L_{STS} training sequence of a ODDM frame to locate the frame boundary. Fig. 3 illustrated the structure of the synchronization sequence in the proposed system. The proposed synchronization sequence uses a pair of identical training sequences, namely 'STS', to perform cross-correlation. Such a synchronization approach is known as the Schmidl and Cox method [12].

3) Channel estimation and equalization: Denoted by $\hat{r}_{\mathbf{sync}}[k] = \hat{r}_{\mathbf{b}}[k+d^*]$ the output of the synchronization process, where d^* is the estimated sample offset from the frame boundary. Assume perfect synchronization is achieved, and hence $\hat{r}_{\mathbf{sync}}[0]$ is the first sample of the CP. The DD-domain channel estimation method proposed in [13] is then considered after the CP is removed.

For $0 \le n \le N-1$ and $0 \le l \le L_z$, we regard $h_l[nM+l]$ as pilot subchannels, which can be independently extracted from the received signal using single-tap equalization

$$\hat{h}_l[nM+l] = \frac{\hat{r}_{\mathbf{sync}}[nM+l]}{\tilde{x}_p[0,n]}, \quad (16)$$

where $\tilde{x}_p[0,n] = \frac{1}{\sqrt{N}} \sum_{\bar{n}=0}^{N-1} X[0,n] e^{j2\pi \frac{n\bar{n}}{N}}$ is the ODDM pilot symbol in time-domain.

The flow of the channel estimation process is illustrated in Fig. 4. First, performing an N-point DFT on the sequence $\hat{h}_l[nM+l]$, for $0 \le n \le N-1$ and $0 \le l \le L_Z$, we have

$$\hat{H}_l[\bar{n}] = \frac{1}{\sqrt{N}} \sum_{n=0}^{N-1} \hat{h}_l[nM+l] e^{-j2\pi \frac{n\bar{n}}{N}} \quad (17)$$

for $\bar{n} = 0, 1, \cdots, N-1$.

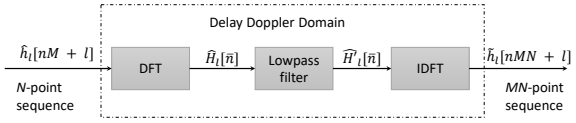

Fig. 4. Channel estimation for the ZP-ODDM system

Since only the Doppler domain channel taps within the range $-\bar{n}_{\nu_{max}} \leq \bar{n} \leq \bar{n}_{\nu_{max}}$ are considered, where $\bar{n}_{\nu_{max}} \leq (N-1)/2$, the channel taps outside the range are lowpass filtered by simply nullifying the high Doppler taps of $\hat{H}_l[\bar{n}]$, which gives

$$\hat{H'}_l[\bar{n}] = \begin{cases} \hat{H}_l[\bar{n}] & 0 \leq \bar{n} \leq \bar{n}_{\nu_{max}}, N-\bar{n}_{\nu_{max}} \leq \bar{n} \leq N-1 \\ 0 & \bar{n}_{\nu_{max}} < \bar{n} < N-\bar{n}_{\nu_{max}} \end{cases}. \tag{18}$$

Note that $\hat{H'}_l[\bar{n}]$ gives an estimation of the channel on the $(l,\bar{n})$-th DD grid. By applying IDFT to the estimated DD domain channel, an estimation on the time domain equivalent channel $\hat{h}'_l[k]$ can be obtained.

4) Iterative successive interference cancellation (SIC) detection: For the proposed zero-padded ODDM system, time-domain iterative SIC method is considered for detecting the transmitted symbols from the received signals. The linear input-output relation for signals in the time domain can be expressed in the matrix format of

$$\mathbf{r} = \mathbf{H}\mathbf{s} + \mathbf{z}, \tag{19}$$

where $\mathbf{r}, \mathbf{s}, \mathbf{z}$ are complex vectors of length MN, representing the received signal, transmitted signal and the AWGN noise in the time domain. The time domain channel matrix $\mathbf{H}$ is a band diagonal matrix of size $MN \times MN$, where the band-width is L_Z+1 which should be greater than the maximum delay-spread of the channel. Furthermore, the ODDM zero symbols padded at the end of the data blocks in the DD domain act as guard bands of length L_Z in the time domain signal $\mathbf{s}$ avoiding interferences between adjacent time domain blocks $\mathbf{r}_n$ for $n = 0, 1, \ldots, N-1$. This implies that the band-diagonal matrix $\mathbf{H}$ can be partitioned into a block-diagonal matrix of N sub-blocks $\{\mathbf{H}_0, \mathbf{H}_1, \cdots, \mathbf{H}_{N-1}\}$, each of size $M \times M$. This enables parallel processing for the detection. Fig. 5 shows the structure of the time domain channel matrix $\mathbf{H}$.

The detection process performes simultaneously in each sub-block $\mathbf{H}_n, 0 \leq n \leq N-1$, in a sliding window manner. The size of the window $\mathbf{w}_j, 0 \leq j \leq M_d - 1$, is $(L_Z+1) \times (L_Z+1)$. The window slides from the top left-hand coner to the bottom right coner to perform symbol-by-symbol detection. Take $\mathbf{H}_0$ in Fig. 6 as an example. The time domain received signal $\tilde{\mathbf{r}}_n$, $0 \leq n \leq N-1$, after interference cancellation corresponding to $\mathbf{w}_j$-th window, $0 \leq j \leq M_D - 1$, is given as

$$\tilde{\mathbf{r}}_n[j : j+L_Z] =$$

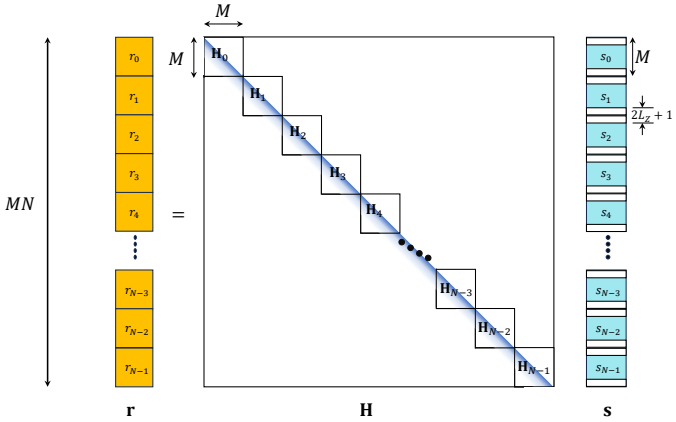

Fig. 5. Time domain input-output relation.

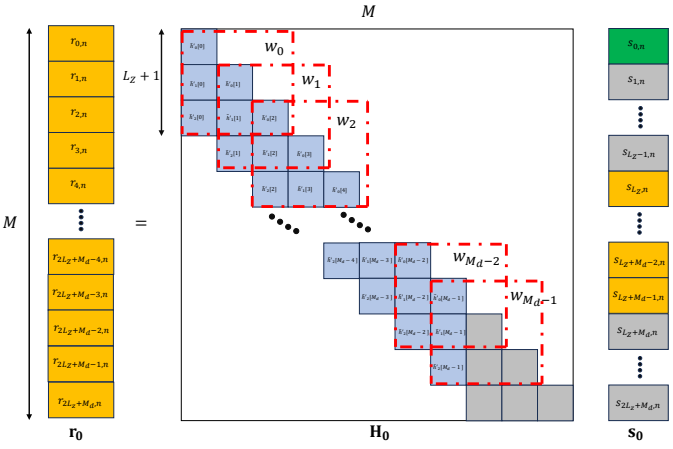

Fig. 6. Time domain input-output relation of sub-block $\mathbf{H}_0$.

$$\mathbf{r}_n[j : j+L_Z] - \sum_{m=0}^{j-1} \mathbf{w}_m[:,m]\hat{s}^{(i)}_{m,n} - \sum_{m=j+1}^{j+L_Z} \mathbf{w}_m[:,m]\hat{s}^{(i-1)}_{m,n}, \tag{20}$$

where $\mathbf{r}_n[j : j+L_Z]$ is the received symbols from j to $j+L_Z$, and $\mathbf{w}_m[:,m]$ denotes the m-th column of window $\mathbf{w}_m$. Furthermore, $\hat{s}^{(i)}_{m,n}$ are the symbols updated in the i-th iteration and $\hat{s}^{(i-1)}_{m,n}$ are the symbols that were estimated in the previous iteration. Hence, the estimation of symbol $\tilde{s}_{m,n}$ is given by

$$\tilde{s}_{m,n} = \boldsymbol{\theta}_{m,n}\tilde{\mathbf{r}}_n, \tag{21}$$

where $\boldsymbol{\theta}_{m,n}$ is some detector used to perform the symbol estimation.

a) MMSE detector: For MMSE detector, we have [2]

$$\tilde{s}_{m,n} = \boldsymbol{\theta}^{MMSE}_{m,n}\tilde{\mathbf{r}}_n, \tag{22}$$

where

$$\boldsymbol{\theta}^{MMSE}_{m,n} = \mathbf{h}^H_m[\mathbf{w}_m\mathbf{V}_m\mathbf{w}^H_m + \sigma^2\mathbf{I}]^{-1}, \tag{23}$$

where $\mathbf{V}_m$ is the covariance matrix of the symbol estimated, which is a constant diagonal matrix, $\mathbf{V}_m = \text{diag}[0, \cdots, 0, E_s, 0 \cdots, 0]$ if hard-decision symbol estimate is

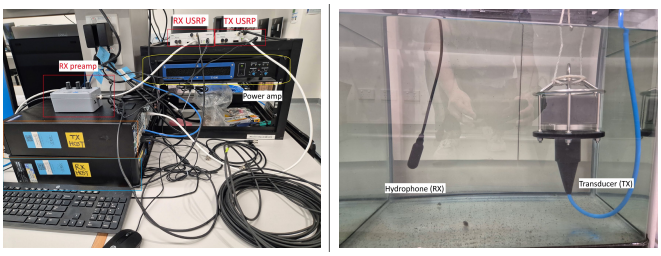

Fig. 7. UWA communication system lab setup.

considered, where E_s is the symbol energy. Here, $\mathbf{h}_m$ is the first column of window $\mathbf{w}_m$, σ^2 is the noise variance, and $(\cdot)^H$ denotes the Hermitian operation.

5) MRC detector: For MRC detector [14], we have

$$\widetilde{s}_{m,n} = \boldsymbol{\theta}_{m,n}^{MRC} \tilde{\mathbf{r}}_n, \tag{24}$$

where

$$\boldsymbol{\theta}_{m,n}^{MRC} = \frac{\mathbf{h}_m^H}{\mathbf{h}_m^H \mathbf{h}_m}, \tag{25}$$

Since there are N sub-blocks perform simultaneouse detection, an estimate of $\tilde{\mathbf{s}}_m = \{\tilde{s}_{m,0}, \tilde{s}_{m,1}, \cdots, \tilde{s}_{m,N-1}\}$ is obtained. Performing N-point DFT on $\tilde{\mathbf{s}}_m$, we have the estimated symbol vector $\tilde{\mathbf{x}}_m$ in DD domain, that is

$$\tilde{\mathbf{x}}_m = \mathbf{F}_N \tilde{\mathbf{s}}_m. \tag{26}$$

The hard-decision detection of the symbol in DD domain is then given by

$$\hat{x}_m[n] = \arg\min_{a_j \in \mathcal{C}} |a_j - \tilde{x}_m[n]|, \tag{27}$$

where $a_j, j = |\mathcal{C}|$ are the points in the constellation $\mathcal{C}$. The hard-decision symbols $\hat{\mathbf{x}}_m = \{\hat{x}_m[0], \hat{x}_m[1], \cdots, \hat{x}_m[N-1]\}$ is transformed back to time domain through an N-point IDFT operation

$$\hat{\mathbf{s}}_m = \mathbf{F}_N^{\dagger} \hat{\mathbf{x}}_m. \tag{28}$$

Note that $\hat{\mathbf{s}}_m$ is the estimate in time domain for the m-th delay, and will be subtracted as interference in the next iteration of detection.

IV. Experimental Setup and Results

In this section, we investigate the performance of our SDR-based ODDM system in a multipath channel environment in a water tank. The setup of the system is shown in Fig. 7. The National Instrument (NI) LabVIEW software environment performs signal generation and processing on the host computers. The SonoTube-008 transducer is connected to the TX port of N210 USRP through a power amplifier and an impedance-matching network for transmitting underwater acoustic signals. At the receiver side, the HTI-96 mini hydrophone is connected to the RX port of another N210 USRP through the RESON EC6081 preamplifier for receiving underwater acoustic signals. The distance between the transducer and the hydrophone is 0.5 meter.

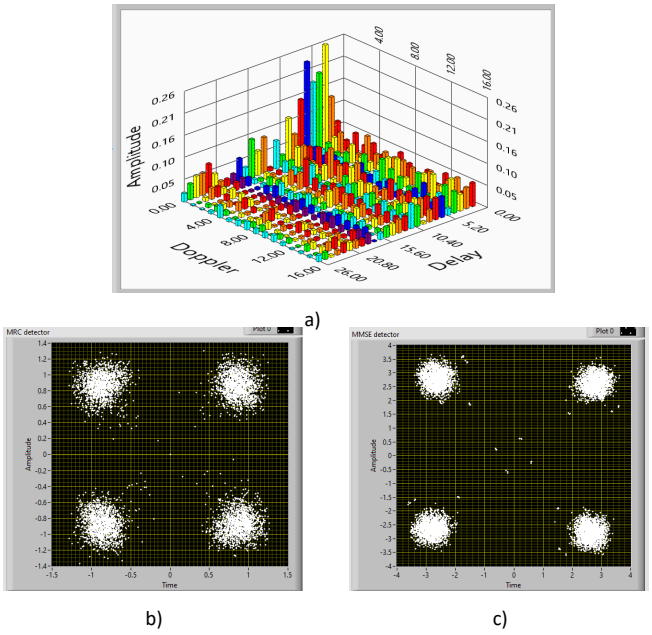

Fig. 8. SDR based ODDM system performance in laboratory water tank. a) DD domain channel impulse response on the DD grid with $0 \leq n \leq N-1$ and $0 \leq m \leq L_Z + 1$ for the Doppler and delay axes, respectively. b) Output of the MRC detector. c) Output of the MMSE detector.

Fig. 8 shows the DD domain channel impulse response, as well as the performance of the MRC and MMSE detectors. The parameters of the ODDM system are as follows:

- Bandwidth $= 4kHz$,
- $f_c = 12kHz$,
- $N = 16$,
- $M = 512$,
- $L_Z = 32$,
- $M_P = 1$,
- $L_b = 14304$,
- Detection iterations= 20.

It can be seen from Fig. 8-a) that since both the transmitter and the receiver are stationary in the water tank, there isn't much Doppler effect. Hence, there are only paths at zero Doppler corresponding to the time domain channel delay profile. 8-b) and c) show the scatter plot of the output of the MRC and MMSE detectors. It can be seen that the MMSE detector shows better performance at a cost of high processing complexity. Although, QAM symbols for both detectors outputs are properly aggregated into the normalized modulation constellations, the output of MMSE shows a constant phase shift compared to the outputs of MRC detector.

Fig. 9 shows the performance of an OFDM system. Since the channel has not changed, the time domain channel impulse response shown in Fig. 9-a) is very similar to the DD domain channel impulse response shown in, 8-a). For comparison, the parameters of the OFDM systems are:

- Bandwidth = $4kHz$,
- $f_c = 12kHz$,
- $FFT = 512$,

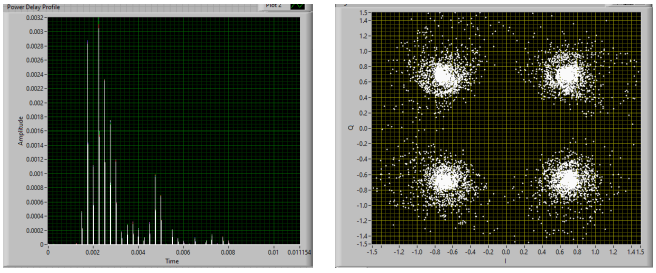

a) b)

Fig. 9. SDR based OFDM system perfromance in laboratory water tank. a) Time domain chanel impulse response. b) Output of the MMSE equalizer

- $N_{pilots} = 64$,
- $N_{null} = 8$,
- $CP = 32$,
- $L_b = 14080$.

Note that the OFDM systems requires N_{pilots} pilot tones and N_{null} null tones inserted in each OFDM symbol for the purpose of channel estimation and carrier frequency offset corrections. In addition, CP is added for each OFDM symbol, which corresponds to the L_Z zeros padded at the end of 2D ODDM frame. The bandwidth effeciency of OFDM system is $(512 - 64 - 8)/512 = 440/512 = 0.86$, whereas for the ODDM system the bandwidth effeciency is $(512 - 2L_Z - 1)/512 = 447/512 = 0.873$. Moreover, since only one CP is added per ODDM frame, the frame duration[2] of ODDM is $(512 * 16 + 32)/BW = 8224/4000 = 2.056$ sec. On the other hand, the frame duration of OFDM system is $(512 + 32) * 16/4000 = 8704/4000 = 2.176$ sec. The bit rate of the ODDM system is 6.96 kbps if 4QAM constellation is considered. The bit rate of the OFDM system is 6.47 kbps. Thus, the ODDM system has a higher bit rate than OFDM system with similar configurations. In order to achieve the similar performance, the ODDM system has a higher receiver complexity compared to the OFDM system. This is mainly due to the complexity of iterative SIC detection process used in the ODDM system, which is much time consuming compared to the single-tap equalizer used in the OFDM system.

V. Conclusions

In this work, the prototype of an ODDM test-bed was implemented using USRP SDR platforms. The frame structure, transmitter process and the receiver process are investigated and illustrated. The performance of the designed ODDM system is comparable to OFDM system for higher bit rate and bandwidth efficiency, while the complexity of detection process is much higher than the OFDM system.

[2]Here, only the size of data frame is considered. The same training sequence, preamble and postamble sequences are applied to both systems.

References

[1] R. Hadani, S. Rakib, M. Tsatsanis, *et al.*, "Orthogonal time frequency space modulation," in *2017 IEEE Wireless Communications and Networking Conference (WCNC)*, 2017, pp. 1–6.

[2] Q. Li, J. Yuan, and H. Lin, "Iterative mmse detection for orthogonal time frequency space modulation," in *2022 IEEE International Conference on Communications Workshops (ICC Workshops)*, 2022, pp. 01–06.

[3] H. Lin and J. Yuan, "Orthogonal delay-doppler division multiplexing modulation," *IEEE Transactions on Wireless Communications*, vol. 21, no. 12, pp. 11 024–11 037, 2022.

[4] A. Shafie, J. Yuan, P. Fitzpatrick, T. Sakurai, and Y. Fang, "On the coexistence of otfs modulation with ofdm-based communication systems," *IEEE Transactions on Communications*, pp. 1–1, 2024.

[5] J. Tong, J. Yuan, H. Lin, and J. Xi, "Orthogonal delay-doppler division multiplexing (oddm) over general physical channels," *IEEE Transactions on Communications*, pp. 1–1, 2024.

[6] H. P. H. Shaw, J. Yuan, and M. Rowshan, "Delay-doppler channel estimation by leveraging the ambiguity function in ofdm systems," in *2023 IEEE International Conference on Communications Workshops (ICC Workshops)*, 2023, pp. 307–313.

[7] K. Huang, M. Qiu, J. Tong, J. Yuan, and H. Lin, "Performance of orthogonal delay-doppler division multiplexing modulation with imperfect channel estimation," *IEEE Transactions on Communications*, pp. 1–1, 2024.

[8] Y. Xue and Y. R. Zheng, "Orthogonal time-frequency space (otfs) modulation for underwater mobile acoustic communications," *The Journal of the Acoustical Society of America*, vol. 154, 2023.

[9] P. Chen, Y. Rong, S. Nordholm, and Z. He, "An underwater acoustic ofdm system based on ni compactdaq and labview," *IEEE Systems Journal*, vol. 13, no. 4, pp. 3858–3868, 2019.

[10] C. Zhang, Y. Xie, D. Mishra, *et al.*, "A low complexity channel emulator for underwater acoustic communications," 2023, pp. 1–8.

[11] T. Thaj and E. Viterbo, "Otfs modem sdr implementation and experimental study of receiver impairment effects," in *2019 IEEE International Conference on Communications Workshops (ICC Workshops)*, 2019, pp. 1–6.

[12] T. Schmidl and D. Cox, "Robust frequency and timing synchronization for ofdm," *IEEE Transactions on Communications*, vol. 45, no. 12, pp. 1613–1621, 1997.

[13] C. Shen, J. Yuan, Y. Xie, and H. Lin, "Delay-doppler domain estimation of doubly-selective channels in single-carrier systems," in *GLOBECOM 2022 - 2022 IEEE Global Communications Conference*, 2022, pp. 5941–5946.

[14] T. Thaj and E. Viterbo, "Low complexity iterative rake decision feedback equalizer for zero-padded otfs systems," *IEEE Transactions on Vehicular Technology*, vol. 69, no. 12, pp. 15 606–15 622, 2020.